Title
The Neutron-Proton Interaction

Authors
Christian, Richard S.
Hart, Edward W.

Publication Date
1949-06-29

UNIVERSITY OF CALIFORNIA

Radiation Laboratory

BERKELEY, CALIFORNIA

DISCLAIMER

UCRL-384
No Distribution
Copy -2.

UNIVERSITY OF CALIFORNIA

Radiation Laboratory

UNCLASSIFIED

Contract No. W-7405-eng-48

The Neutron-Proton Interaction

Richard S. Christian and Edward W. Hart

June 29, 1949

Berkeley, California

The Neutron-Proton Interaction

Richard S. Christian and Edward W. Hart

Radiation Laboratory and Department of Physics

University of California

Berkeley, California

June 29, 1949

Introduction

The purpose of the present paper is to ascertain if it is possible to determine a phenomenological description of the neutron-proton interaction in terms of a potential. A further aim is to determine with what uniqueness this potential can be determined from the present experiments, particularly those at high energies. The program will be to assume a number of potential models so adjusted that they fit the low energy region and attempt to correlate the high energy scattering with the various features of each model.

It is well known that the experimental results in the low energy region can be described by an interaction potential; however, for sufficiently high energies relativistic corrections may be expected to be of major importance. Detailed scattering calculations, using a field theory, show that the use of relativistic momenta corresponds to calculating the kinematical aspects relativistically, but that the dynamical corrections depend on the specific theory employed. Scattering deduced from a field theory[1] has, in general, relativistic correction proportional to $(v/c)^2$; for example, at 90 Mev $(v/c)^2$ is 0.05 while approximately 10 percent corrections are found by application of the Moller method to the scalar and

vector meson theories.(2) Thus a choice cannot be made between two models both of which agree within 10 percent with the experimental results at 90 Mev.

The experimental data which will be considered are presented in Table 1 and 2 and in Fig. 1. (The magnetic dipole moment is not fitted because of uncertain relativistic corrections.)

The binding energy and low energy scattering experiments including the coherent scattering amplitude yield no information on the explicit shape of the potential but do serve to determine the triplet depth and effective range. The singlet state depth is accurately determined from the zero energy cross section because of the proximity of a virtual level, but the singlet range cannot be determined with nearly the same accuracy.

A unique analysis of the experimental angular distribution is impossible due to the presence of the mixture of singlet and triplet states as well as the complication of the tensor force. Nevertheless, on the simplifying assumption of scattering with no spin dependence, the 90 Mev angular distribution may be analyzed to give the order of magnitude of the phase shifts. The results of this are: S-wave, $53^\circ \pm 5^\circ$; P-wave, $-1^\circ \pm 1^\circ$; D-wave, $5^\circ \pm 1^\circ$. Since the P and D phase shifts are so small, we may conclude that at 90 Mev the S scattering accounts for about 90 percent of the total scattering cross section. The high energy cross sections, therefore, determine the S scattering fairly unambiguously. The potentials usually considered show significant differences in S scattering above 30-40 Mev when adjusted to have the same low energy properties. The comparison then of the S-wave cross sections provides one method of determining the potential shape.

The angular distribution at a particular energy yields information primarily concerning the exchange character of the forces. For example,

The desired representation of the solutions is then

$$u = \cos \eta \sqrt{\frac{S}{S'}} Z_{1/3}(S)$$

$$w = \sin \eta \sqrt{\frac{S}{S'}} Z_{1/3}(S)$$

where

$$(S_{\pm}')^2 = \frac{1}{2}\left\{A + C \pm \sqrt{(A - C)^2 + 4B^2}\right\}$$

$$\tan \eta = (S_{\pm}'^2 - A)/B$$

The + and - signs correspond to two independent representations. The Z's are Bessels functions of order 1/3. The usual phase integral condition for the bound state is replaced by the similar condition,

$$\int_{x_1}^{x_2} S'dx = S_n$$

where x_1 and x_2 are the turning points and S_n is a root of

$$\frac{d}{dS}\sqrt{S}\left[J_{1/3}(S) + J_{-1/3}(S)\right] = 0$$

These representations have been found to yield close approximations to the wave functions at all energies, the S-wave phase shifts being in general in error by less than five degrees, and the wave functions exhibiting the correct general behavior. When applied to the bound state, the phase integral condition yields potential depths that are within 10 percent of the correct value.

The $^3S_1 + {}^3D_1$ state required in general about three iterations to achieve an accuracy of about 1 percent. The accuracy was limited essentially by the numerical methods used. The higher state required only one iteration.

The Born approximation was used to effect the inclusion of the angular momentum states for $\ell \geq 4$ in the scattering sum. The sum was, in general,

done by actually summing the individual terms for $\ell \leq 3$, using calculated phase shifts, and adding the Born cross section from which these states had been suitably subtracted. The angular distribution so derived are accurate within 2-5 percent.

Central Forces

We shall consider in this section the results of scattering from a model which consists only of central forces since, as will be seen later, it is possible to make a state by state comparison of the scattering from a central force model and from one which includes tensor forces.

The details of low energy scattering will not be treated here, but, rather, the reader is referred to the review of Blatt and Jackson.(16) The main result of that work is that the shape dependent coefficient in the expansion of k cot δ (i.e., the coefficient of the square of the energy) is sufficiently small that below 6 Mev it can be neglected, and, in interpreting the experiments, the shape independent approximation may be used. The effective range in the triplet state is determined, therefore, by the approximate relation

$$\frac{1}{^3a} = -\frac{1}{r_d}\left(1 - \frac{1}{2}\frac{^3r}{r_d}\right)$$

Substituting the experimental values from Appendix I, we obtain

$$^3r = 1.53 \pm .20 \times 10^{-13} \text{ cm.}$$

Fig. 2 is a plot of effective range versus intrinsic range for the triplet state of the various potentials. The singlet effective range is not well determined by the present experiments, as can be seen by reference to Figs. 3 and 4.

To simplify the analysis of the high energy data, it is convenient (and reasonable) to assume exact symmetry of scattering about 90 degrees. This means that the potential is assumed to be zero in odd parity states. The

experimental results are actually compatible with a small repulsive potential in odd states, but this shall be considered as a small perturbation which will not essentially alter any of the following conclusions. The factor $1/2\ (1 + P_x)$ will, therefore, be included in the potential and will have as one consequence that the total cross section computed for any potential radial dependence will be the minimum possible over any choice of exchange dependence. The main effect of any admissible odd wave phase shifts is the interference with the large S-wave phase shift, which is in evidence only in the angular distribution, and its actual effect on the total cross section is negligible.

In order to compare different potential shapes, the effective range has been taken as a common parameter. For example, we have plotted (Fig. 5) the S-wave phase shift at 90 Mev for the various potentials versus the effective range. This device insures similar low energy behavior for the same abscissa.

In Fig. 6 are plots at 90 Mev for the various potentials of the total cross section and of 4π times the differential cross section for scattering at 90° and 180° as functions of the effective range on the assumption of no odd parity interaction. For the plots of complete total cross section, i.e., the sum of triplet and singlet scattering, it is necessary to make some choice of a singlet range corresponding to a particular triplet range. The low energy region implies only loose restrictions on the singlet range; we may, therefore, choose the singlet range so that the singlet and triplet intrinsic ranges are equal. The results for the complete cross sections are also shown in Fig. 6. From these plots it is possible to make further limitations on the allowable triplet ranges by a comparison with the experimental values of $\frac{\sigma(180)}{\sigma(90)}$.

With the Yukawa or exponential potential a range adjusted for the 90

Mev ratio predicts a 40 Mev ratio within the experimental limits. However, with the square well potential, the range required at 40 Mev is considerably larger than that required at 90 Mev. This difference in behavior results primarily from the more rapid decrease in $\sigma(90^{o})$ with energy increase for the "cut-off" potential than for the "long-tailed" potentials. This, in turn, can be interpreted in terms of the destructive interference between the S and D waves at 90 degrees. In detail, the S-wave phase shift decreases more rapidly (as a function of energy) for the "cut-off" potentials (Fig. 7). Further the D-wave phase shift increases more rapidly for the "cut-off" potentials (Fig. 8).

Potentials which have a "deep hole" at the origin (e.g., the Yukawa and exponential) the "long-tail" is necessary to give a sufficiently long effective range. However, as the energy increases the contributions to the S-wave phase shift come from regions closer to the origin, and, consequently, at high energies the "deep hole" (and, therefore, "long-tailed") potentials yield larger phase shifts than the "cut-off" potentials (e.g., the square well or gauss potentials). These remarks are further illustrated by reference to Figs. 5 and 7.

While it is impossible to define the limits of the singlet effective range with any accuracy, for $^{3}r < 1.7 \times 10^{-13}$ cm the best fits for the angular distribution are obtained with the singlet effective range between $2.5 - 3.0 \times 10^{-13}$ cm.

The measured total cross sections are in better agreement with the larger singlet range, above, since decreasing the range to 1.0×10^{-13} increases the theoretical cross section by 10 percent at both 40 and 90 Mev.

The complete calculated angular distributions for a number of the more favorable cases are shown in Fig. 9 and 10. Fig. 9 also shows the effect of adding a small repulsive potential in the odd parity states. This modifica-

tion may be expressed by a potential factor, $(1 - a + aP_x)$. The best fit for this type of interaction is $a = 0.55 \pm 0.05$.

The large odd state potentials in the singlet state required by the symmetrical theory produces far too much exchange scattering for any potentials with a tail and a range compatible with low energy scattering. For "cut-off" potentials such as the square well the observed ratio $\frac{\sigma(180^\circ)}{\sigma(90^\circ)}$ may be fitted at 90 Mev with a range of $1.7 - 1.8 \times 10^{-13}$ cm; however, at 40 Mev, a fit to $\frac{\sigma(180^\circ)}{\sigma(90^\circ)}$ would require a range longer than 2.0×10^{-13} cm. Furthermore, in these latter cases the shape of the predicted angular distribution is not similar to the experimental results for small angle scattering. The symmetrical theory can, therefore, be ruled out for central forces.

Tensor Forces

A. General considerations

The existence of the deuteron quadrupole moment requires the inclusion of a tensor potential in the neutron-proton interaction.

The calculations of Rarita and Schwinger[20] have shown that at least for the choice of a square potential, there is only slight modification of the low energy scattering properties upon the introduction of tensor forces. Such a behavior can be expected for more general potential shapes with ranges shorter than the deuteron radius since the S-wave component is determined primarily from the boundary conditions at the origin and asymptotically.[21]

We can put these arguments on a quantitative basis by the consideration of an "equivalent central potential," "V(r)." For the potential $V(r) = V_c(r) + \gamma S_{12} V_t(r)$, "The equivalent central potential for the S-wave is

$$"V(r)" = V_c(r) + 2^{3/2} \gamma V_t(r) \cdot R(r) ,$$

where R(r) is the ratio of the D-wave to the S-wave, R(r) will be, in general, a slowly varying function of the energy (at least in the region where the potential is large). Its form may then be estimated from considerations of the bound state solutions. It is found then that R(r) is zero at the origin, increases to a maximum value (about 0.2 or 0.3) somewhere between the maximum of the S-wave radial function and the tensor force range, and decreases asymptotically to a small value (somewhere under 0.1). Then if we consider the ratio of the equivalent potential "V(r)" to the central potential $V_c(r)$ (the latter adjusted to give binding by itself), we would find the ratio to be less than unity at the origin, greater than unity in the neighborhood of the range, and again less than unity asymptotically. Thus the equivalent potential will be shallower at the origin and asymptotically, and will be deeper in the neighborhood of the tensor range.

This can be further illustrated in terms of the WKB approximation. In this approximation, R(r) is independent of energy and decreases asymptotically to zero. The equivalent potential in this approximation is

$$"V" = V_c - \gamma V_t - \frac{3}{x^2} + \sqrt{(\gamma V_t + \frac{3}{x^2})^2 + 8 (\gamma V_t)^2}$$

If the centrifugal potential is large compared to the tensor potential, this may be simplified to

$$"V" = V_c + \frac{4}{3} (\gamma x V_t)^2$$

which is clearly in agreement with the preceding remarks.

B. Bound state and low energy scattering

We consider first the case where the radial dependence is chosen the same for both the central and tensor potentials. The extreme cases of "long-tailed" and "cut-off" potentials are exemplified by the Yukawa and square wells respectively. Calculations of the quadrupole moment have been made

for these two potentials as a function of range and tensor depth with the central depth adjusted to give the correct binding energy. The results are presented graphically in Figs. 11, 12 and 13.

The analysis of the low energy scattering is again conveniently carried out in terms of the expansion of the phase shift in powers of the energy.(23) Since the shape independent approximation is valid for Yukawa ranges less than 1.4×10^{-13} cm and for all square well ranges considered, the effective range is essentially determined from the triplet scattering length. (The explicit value of the shape dependent coefficient as well as the effective ranges are shown in Table 3 for a number of cases.) We have chosen, therefore, in order to relate the scattering characteristics of a potential with its ability to produce a quadrupole moment, to plot $1/\gamma$ versus the scattering length (Fig. 14) with the range indicated parametrically along the curves. From this plot we can conclude that with the accepted value of the scattering length, the proportion of tensor potential must be quite large, the actual amount being lower for the long-tailed potential.

The effect of increasing the range of the tensor force relative to that of the central force is to enhance the "long-tailed" character of the potential (Fig. 15).

C. High energy scattering

In the case of the central force model the only partial waves contributing appreciably to the cross section are the S- and D-waves. Consequently, the angular distribution can be expanded in terms of the Legendre polynomials P_0, P_2, and P_4. The coefficient of P_0 is identical with the total cross section, that of P_2 arises primarily from interference between the S- and D states, and that of P_4 arises from combination of the various D states. A similar situation can be expected to hold for the tensor force.

Using the WKB approximation we can evaluate the "equivalent central potentials," "V_L^J", for each of the states of L and J, with the result

$$"V_0^1" = V_c - \gamma V_t - \frac{3}{x^2} + \left[\left(\frac{3}{x^2} + \gamma V_t\right)^2 + 8(\gamma V_t)^2\right]^{1/2} \times V_c + \frac{4}{3}(\gamma \times V_t)^2$$

$$"V_2^1" = V_c - \gamma V_t - \frac{3}{x^2} - \left[\left(\frac{3}{x^2} + \gamma V_t\right)^2 + 8(\gamma V_t)^2\right]^{1/2} \approx V_c - 2\gamma V_t + \frac{4}{3}(\gamma \times V_t)^2 - \frac{6}{x^2}$$

$$"V_2^2" = V_c - 2\gamma V_t - \frac{6}{x^2}$$

$$"V_2^3" = V_c - \gamma V_t - \frac{13}{x^2} + \left[\left(\frac{7}{x^2} + \frac{3}{7}\gamma V_t\right)^2 + 3\left(\frac{12}{7}\gamma V_t\right)^2\right]^{1/2}$$

$$\approx V_c - \frac{4}{7}\gamma V_t + \frac{3}{14}\left(\frac{12}{7}\right)^2 (\gamma \times V_t)^2 - \frac{6}{x^2}$$

In the approximation where we neglect the asymptotic amplitude of the coupled mode, as above, in the evaluation of the phase shifts there will be no difference between states of different magnetic quantum number, m_s.

As can be expected on the basis of the "equivalent potentials" there is only a small difference in the total scattering from the $^3S_1$ state, which has been confirmed by actual calculation in a number of cases. Further we can summarize the behavior of the various D states in the following: ($^3D_1$) Increasing the tensor depth (i.e., γ) decreases the equivalent potential and for strong tensor forces the resulting potential will be strongly repulsive. ($^3D_2$) Increasing γ increases the potential depth to such an extent that for equal range central and tensor potentials the depth which gives the quadrupole moment is 3 to 4 times as deep as the depth on the central force model. ($^3D_3$) The potential decreases for increasing γ such that for $\gamma \sim 1$ the potential will be just barely repulsive. Approximately the same effect is achieved by increasing the tensor range instead of the depth.

To illustrate we will consider the high energy scattering from two extreme examples (which do not necessarily fit the low energy scattering but are adjusted for quadrupole moment and binding): (1) the central and

tensor depth are approximately equal with the square well dependence of 2.7 x 10^{-13} cm, (2) the tensor depth accounts for practically all the binding with a Yukawa dependence and range of 1.2 x 10^{-13} cm. In Table 4 we have summarized the contribution of each state to the total cross section and indicated the sign of the phase shift (i.e., the average over m_s). The results of the central force model with the same range and radial dependences are included for comparison.

The results of using a Yukawa radial (Fig. 16 and 17) indicates that the addition of tensor forces causes relatively small changes in the angular distribution. The changes which do occur are such that a slight increase in range is necessary to retain the ratio $\sigma(180^\circ)/\sigma(90^\circ)$.

We can conclude by reference to Fig. 17 that the exchange dependence found necessary for the central force model applies also for the tensor force model. In particular, the symmetrical theory will be unsuitable on the basis of angular distribution as well as the total cross sections.

Utilizing this comparison between the tensor and central force models developed above we can conclude that the potential must be "long-tailed" in order to maintain the relatively large scattering in the D state at 40 Mev without excessively large scattering in the D state at 90 Mev. "Cut-off" (e.g., square and gauss) potentials where the tensor force has nearly the same range as the central force are, therefore, unsuitable. An addition of a long shallow tail (5-6 x 10^{-13} cm) to the square well is required in the central force case to fit the relative 40:90 Mev scattering and would, therefore, also be required for tensor forces. Potentials formed by the addition of such long-tails would seem to be indistinguishable from naturally long-tailed potentials such as the exponential or the Yukawa potential.

A detailed comparison of the angular distribution can be made in terms of the coefficients in the Legendre expansion. The coefficients of P_0 and

P_2 are only slightly altered while the coefficient of P_4 is considerably smaller in the tensor case. The P_0 coefficient can be explained by the relatively small decrease in the scattering from the $^3S_1$ state (even this decrease tends to be compensated by an increase in the $^3D_2$ state). The relative constancy of the P_2 coefficient can be explained by an almost complete lack of interference between the tensor and central scattering. The decrease in the coefficient of P_4 appears to be a tensor phenomenon. It is just this decrease, however, which makes the agreement in the angular distribution better for tensor forces.

The variation in the high energy scattering with increase in tensor force range is illustrated in Fig. 18. As to be expected on the basis of the WKB arguments, the principal effect is identical with an increase in the "long-tailed" character. If the tensor force range is increased (even by as much as a factor of two) the effect may be compensated by a decrease in the central range.

Finally the Yukawa potential because of the singularity at the origin predicts cross sections that are considerably too high for any combination of ranges. The exponential well is, therefore, to be preferred.

Conclusions

1. Exchange character. If the potential has approximately the same radial dependence in all states (i.e., even and odd parity, singlet and triplet) and the range is chosen within acceptable limits, we may conclude that for a good fit

$$a \simeq 0.55 \pm 0.05$$

or, alternatively, the depths of the odd potentials, V_{odd}, must satisfy the relation

$$0 > \frac{1}{4}\,(^1V_{odd}) + \frac{3}{4}\,(^3V_{odd}) < -\frac{1}{5}\,(^3V_{even})$$

2. Radial dependence. The $(1 + P_x)/2$ potentials, compared for equal effective ranges differ by at most a factor of 2 in the total cross section or in the ratio $\sigma(180^\circ)/\sigma(90^\circ)$. However, these differences may be correlated with general shape features. Further the experiments are adequate to distinguish among the potential shapes.

a. A long-tailed potential is necessary to explain the large scattering from the higher angular momentum states at 40 Mev without violently affecting the 90 Mev scattering. On this basis the square and gauss potentials are unacceptable while the exponential and Yukawa potentials are allowable.

b. The Yukawa potential, because of its singular nature, predicts too high total cross sections for any combinations of ranges. The exponential potential for approximately the same angular dependence predicts cross sections 10 percent to 20 percent lower and, therefore, is favored.

The best fit for these potentials is (assuming the same range for all the forces)

$$r = 0.8 \times 10^{-13} \text{ cm} \quad \text{(exponential)}$$

$$r = 1.35 \times 10^{-13} \text{ cm} \quad \text{(Yukawa)}$$

c. The shape of the angular distribution about 90° is evidence of a tensor force in scattering. Here, with a $\frac{1}{2}(1 + P_x)$ dependence, a purely central force yields a flatter distribution than an interaction including tensor force. The latter distribution agrees significantly better with experiment.

3. Singlet Range. The total cross section measurements imply a singlet range greater than 2×10^{-13} cm. A long singlet range is further favored by the angular distribution. Low energy scattering yields only the requirement that the singlet range be less than 3×10^{-13} cm.

4. Triplet Range. The low energy limits on the effective range are

$1.53 \pm .20 \times 10^{-13}$ cm. The determination of the limits on the range from high energy scattering depend upon the explicit model used but has always been found to be within the limits $1.4 - 1.75 \times 10^{-13}$ cm.

5. Tensor Force Range. The tensor range may be increased relative to the central range by as much as a factor of 2 without adversely affecting either the low or high energy results.

Table 1.

Derived Quantities

Quantity	Notation	Magnitude	Source (with error)
singlet scattering length	^1a	$23.70 \pm .10 \times 10^{-13}$ cm	ortho-para scattering[4] ($\pm 0.03 \times 10^{-13}$ cm) crystal-scattering[5] ($\pm 0.05 \times 10^{-13}$ cm) zero energy cross section[6] ($\pm 0.06 \times 10^{-13}$ cm)
radius of deuteron	γ r_d	$4.332 \pm .025 \times 10^{-13}$ cm	directly determined[7] binding energy 2.21 Mev
triplet scattering length	^3a	$5.26 \pm .12 \times 10^{-13}$ cm	ortho-para scattering ($\pm .09 \times 10^{-13}$ cm) crystal scattering ($\pm .15 \times 10^{-13}$ cm) zero energy cross section ($\pm .03 \times 10^{-13}$ cm)
triplet effective range (shape ind. approx.)	^3r	$1.53 \pm .20 \times 10^{-13}$ cm	from ^3a ($\pm .17 \times 10^{-13}$ cm) from r_d ($\pm .03 \times 10^{-13}$ cm)
singlet effective range	^1r	$< 3 \times 10^{-13}$ cm	scattering between 0 and 6 Mev
electric quadrupole moment	Q	$2.73 \pm .05 \times 10^{-27}$ cm^2	directly determined[8]
percent D-state	W_D	3.9 percent	magnetic dipole moment, neglecting relativistic effects

UCRL-364

Table 2.

High Energy Total Cross Sections

Mean energy Mev	Total cross section with statistical error 10^{-24} cm	Detection method	Average $\sin^2 \delta_s$	Ref.
41 ± 4	.174 ± .010	Proton recoils	.67 ± .11	(9)
40 ± 4	.202 ± .007	$C^{12}(n,2n)C^{11}$	.76 ± .11	(10)
83 ± 7	.083 ± .004	$C^{12}(n,2n)C^{11}$	.66 ± .08	(11)
90 ± 3	.079 ± .007	Proton recoils	.68 ± .08	(9)
95 ± 5	.073 ± .002	Bi fission	.66 ± .06	(12)

The error in the mean energy arises from uncertainties in detector efficiency, neutrons beam distribution, and variation of cross section with energy.

The "average" $\sin^2 \delta_s$ is determined by subtracting the contributions of the higher partial waves as derived from the angular distribution on the basis of no spin dependence in scattering.

Table 3.

Properties of Selected Yukawa Potentials

Central range (10^{-13} cm)	Tensor range (10^{-13} cm)	γ	W_D	${}^3\rho$ (10^{-13} cm)	${}^3r$ (10^{-13} cm)	T (10^{-39}cm^3)	${}^3a$ (10^{-13} cm)
1.18	1.18	5.6	5.3	1.56	1.48	.3	5.22
1.18	1.69	0.8	3.2	1.71	1.49	1.0	5.29
1.18	1.98	0.5	2.8	1.76	1.50	1.2	5.30
1.18	3.91	0.16	1.7	1.90	1.45	2.1	5.35
1.18	(No tensor force)	--	--	1.67	1.54	.6	5.29
1.35	1.35	1.91	4.2	1.71	1.58	.55	5.32
1.35	(No tensor force)	--	--	1.85	1.63	.96	5.39

The shape dependent coefficient (T) has been only approximately determined from the difference of the effective ranges, ${}^3\rho$ (using the deuteron wave functions) and ${}^3r$ (using the bound state wave function).

Table 4.

Comparison of Contributions of Various States to Total Cross Section

State	Square well		Yukawa	
	Tensor forces (10^{-26} cm^2)	Central forces (10^{-26} cm^2)	Tensor forces (10^{-26} cm^2)	Central forces (10^{-26} cm^2)
$^3S_1$	2.95^+	3.25^+	8.82^+	9.58^+
$^3D_1$	0.35^-	0.95^+	0.55^-	0.14^+
$^3D_2$	5.87^+	1.58^+	1.82^+	0.24^+
$^3D_3$	0.72^+	2.21^+	0.14^-	0.33^+

References

1. L. Rosenfeld, Nuclear Forces, Vol. 2, Interscience Pub., New York, page 311 et seq. It might appear at first sight that corrections due to spin orbit coupling are of order v/c. Actually in a field theory calculation corrections which introduce this coupling include also a gradient of the potential (e.g., the Thomas term for the hydrogen atom) which in scattering produces an additional factor of v/c.

2. H. Snyder and R. E. Marshak, Phys. Rev. 72, 1253 (1947)

3. R. G. Sachs, Phys. Rev. 72, 91 (1947)
H. Primakoff, Phys. Rev. 72, 118 (1947)
G. Breit and I. Bloch, Phys. Rev. 72, 135 (1947)

4. R. B. Sutton et al., Phys. Rev. 72, 1147 (1947)

5. C. G. Schull et al., Phys. Rev. 73, 842 (1948)

6. W. B. Toner, Jr., Phys. Rev. 74, 364 (1948)
E. Melkonian, L. J. Rainwater, W. W. Havens, Jr., Bull. Am. Phys. Soc. 24, No. 1, Paper G1 (1949)

7. R. E. Bell and L. G. Elliot, Phys. Rev. 74, 1552 (1948)
W. E. Stephens, Rev. Mod. Phys. 19, 19 (1947)
W. E. Stephens, Bull. Am. Phys. Soc. 24, No. 4, Paper T1 (1949)

8. A. Nordsieck, Phys. Rev. 58, 310 (1940)

9. J. Hadley, et al., Phys. Rev. 75, 351 (1949)

10. R. H. Hildebrand and C. E. Leith, Bull. Am. Phys. Soc. 24, No. 6, Paper C8 (1949); also private communication

11. L. J. Cook, et al., Phys. Rev. 72, 1264 (1947)

12. J. DeJuren, N. Knable, and B. Moyer, Bull. Am. Phys. Soc. 24, No. 6, Paper E9 (1949)

13. K. Brueckner, et al., Phys. Rev. 75, 555 (1949)

14. N. Svartholm, "The Binding Energies of the Lightest Atomic Nuclei", Lund (1945)
J. Schwinger, Phys. Rev. 72, 742 A (1947), and hectographed Notes on Nuclear Theory, Harvard (1947)

15. R. E. Langer, Phys. Rev. 51, 669 (1937)

16. J. M. Blatt, Phys. Rev. 74, 92 (1948)
J. M. Blatt and J. D. Jackson, Phys. Rev. (in press)

17. C. D. Bailey, et al., Phys. Rev. 70, 583 (1946)
J. H. Williams, private communication

18. W. Sleator, Jr., Phys. Rev. 72, 207 (1947)

19. R. Sherr, Phys. Rev. 68, 240 (1945)

20. W. Rarita and J. Schwinger, Phys. Rev. 59, 436 (1941)

21. W. Hefner and R. Peierls, Proc. Roy. Soc. 181, 43 (1942)

22. The results for R= 1.185 x 10^{-13} cm are in agreement with those from more precise calculations communicated to the authors by H. Feshbach

23. R. Christian, Phys. Rev. 75, 1675 (1949)

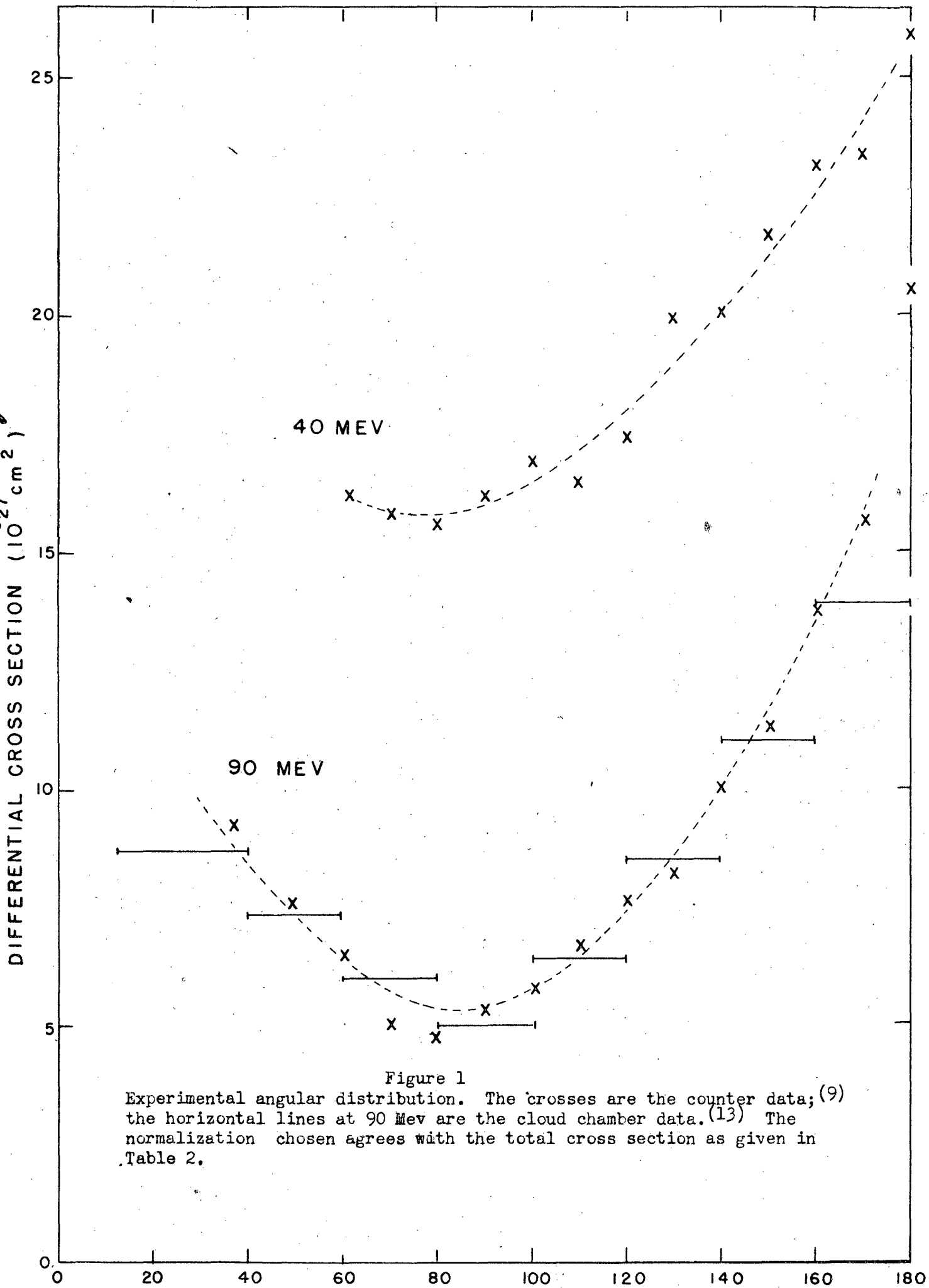

Figure 1
Experimental angular distribution. The crosses are the counter data;[9] the horizontal lines at 90 Mev are the cloud chamber data.[13] The normalization chosen agrees with the total cross section as given in Table 2.

$V = \frac{e^{-r/R}}{r}$. (Yukawa)

choose R

adjust depth for zero energy resonance

then effective range = intrinsic range.

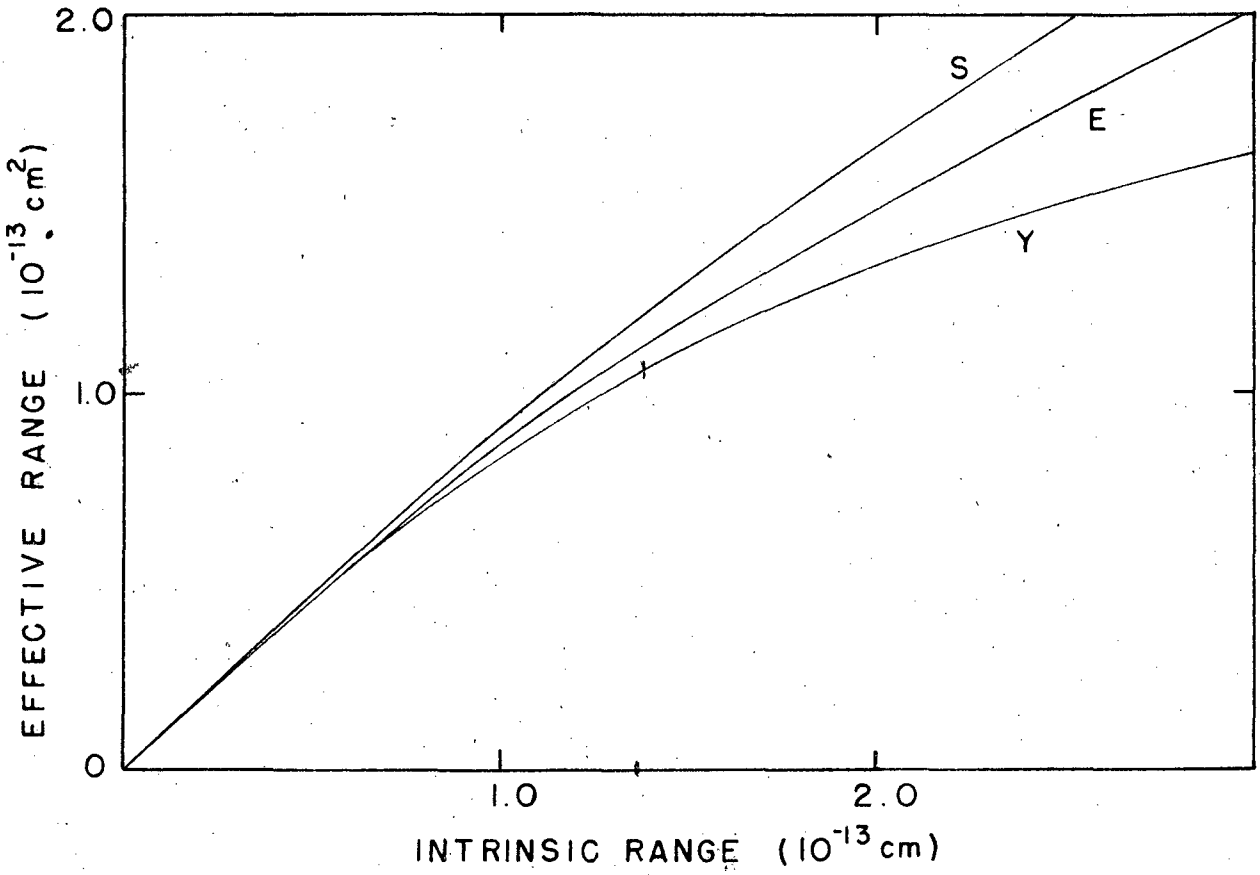

Figure 2
The triplet effective range for the Yukawa (Y), exponential (E), and the square well (S) potentials. The intrinsic range is 2.12 R, 3.54 R, and R for the three potentials in the order named above.

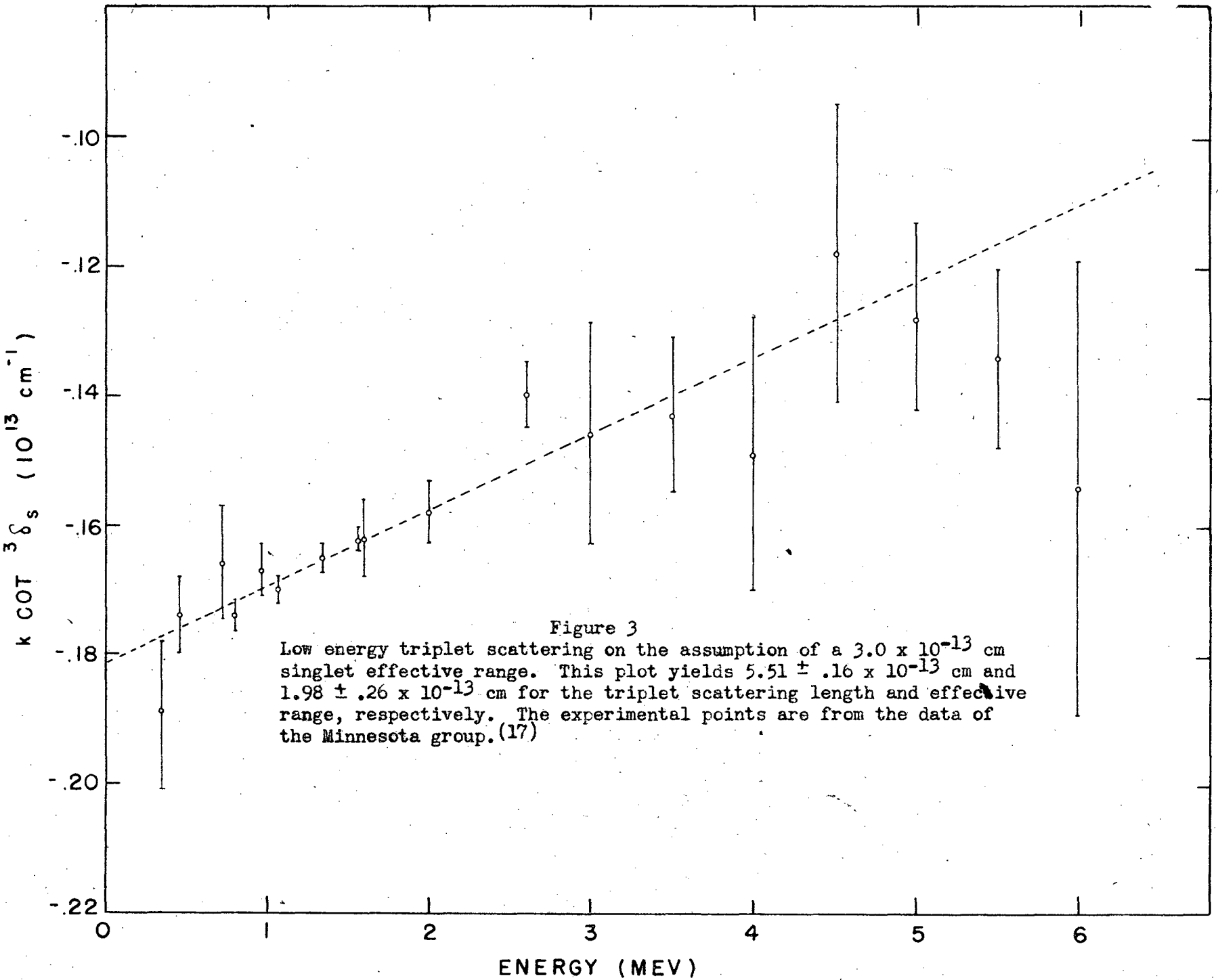

Figure 3

Low energy triplet scattering on the assumption of a 3.0×10^{-13} cm singlet effective range. This plot yields $5.51 \pm .16 \times 10^{-13}$ cm and $1.98 \pm .26 \times 10^{-13}$ cm for the triplet scattering length and effective range, respectively. The experimental points are from the data of the Minnesota group.(17)

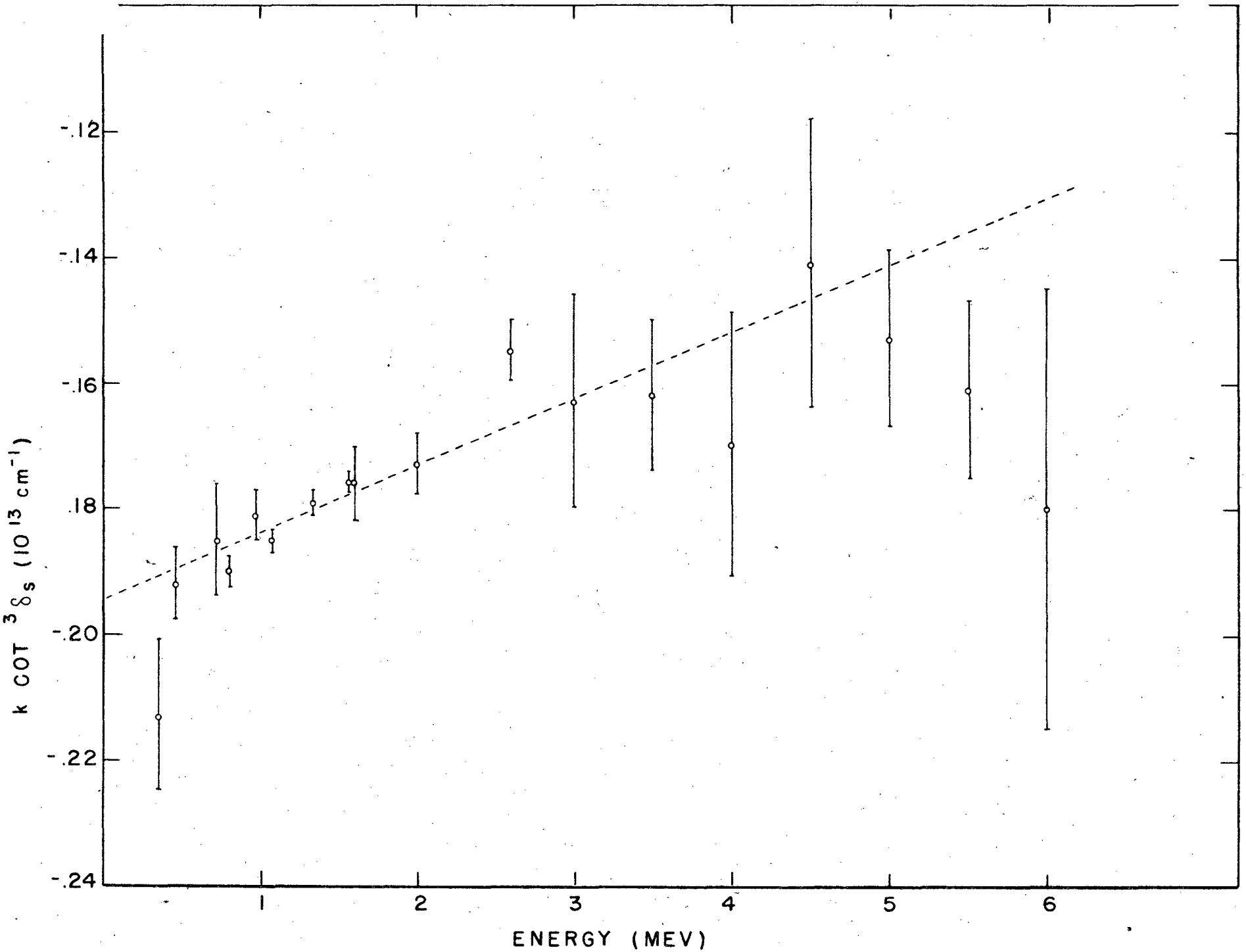

Figure 4

Low energy triplet scattering on the assumption of a zero singlet range. This plot yields $5.14 \pm .16 \times 10^{-13}$ cm and $1.77 \pm .26 \times 10^{-13}$ cm for the triplet scattering length and effective range, respectively.

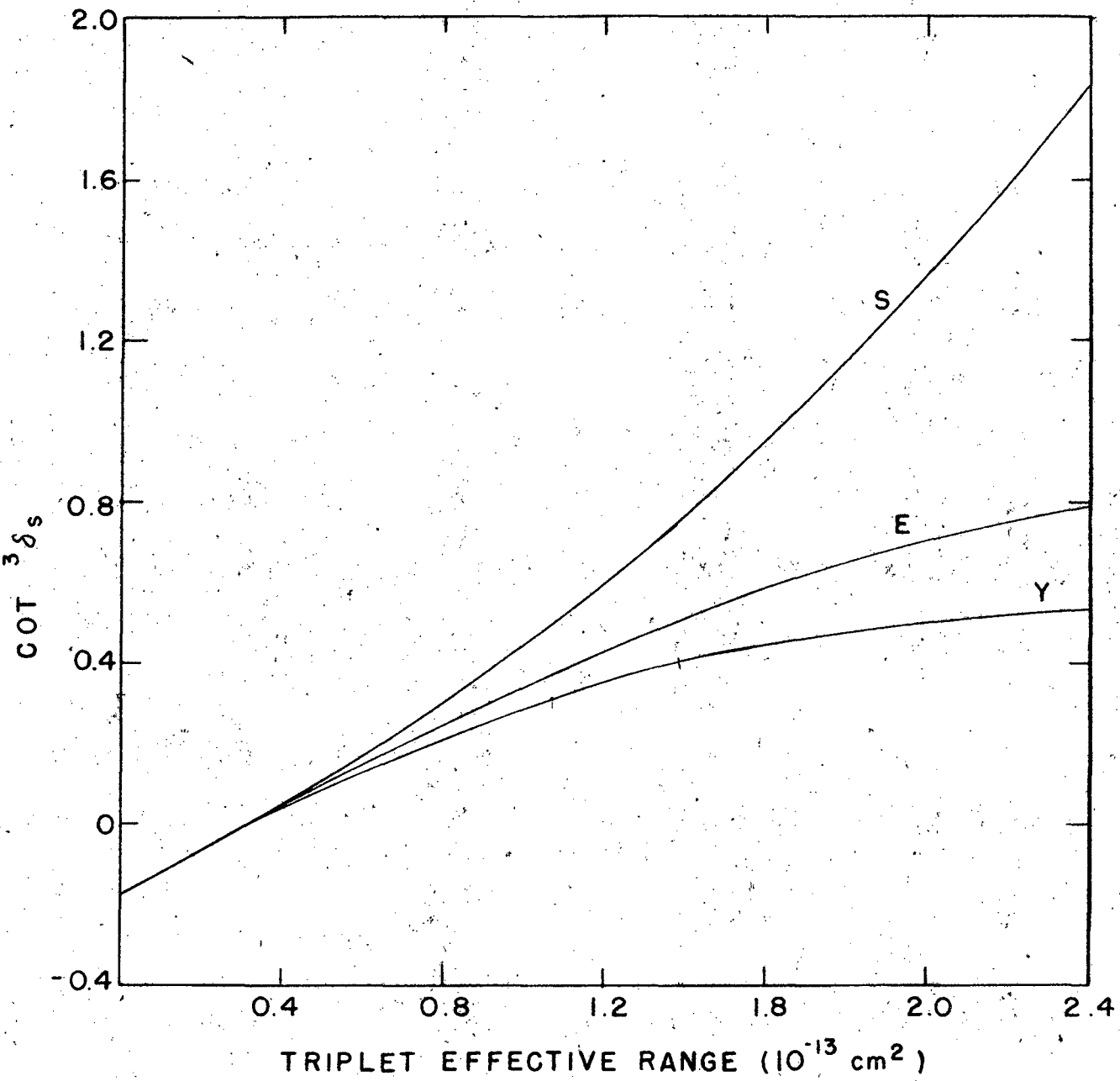

Figure 5
Triplet S-wave scattering at 90 Mev.

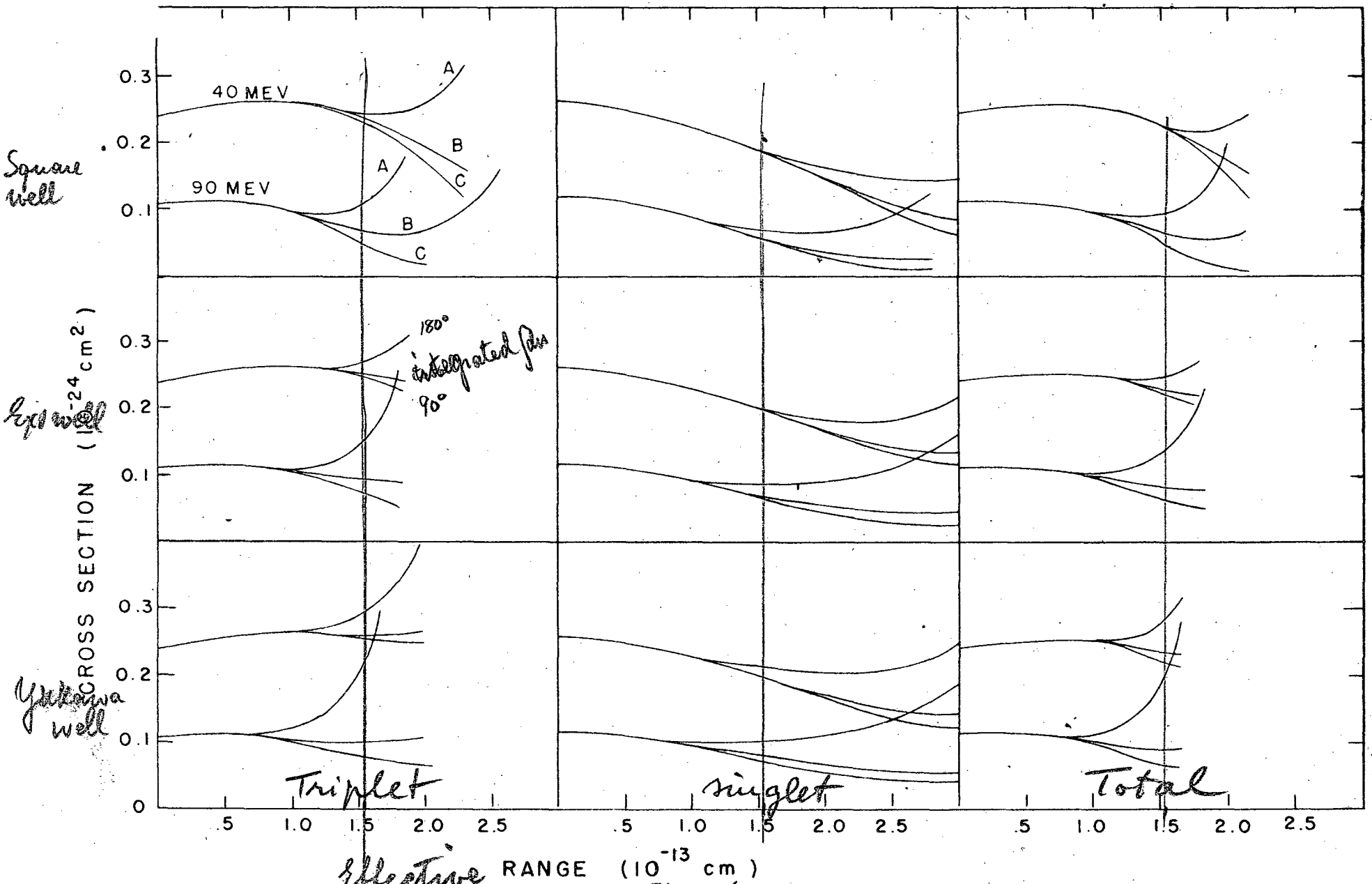

Figure 6

Central force scattering at 40 and 90 Mev. The first column gives the triplet scattering; the second, the singlet scattering; and the third, the complete scattering (assuming equal intrinsic ranges). The first row is for the square well; the second, for the exponential; and the third, for the Yukawa potential. In each figure the upper set of 3 curves is for 40 Mev; the lower, for 90 Mev. For each set of 3 curves the uppermost is $4\pi \cdot \sigma(180^\circ)$; the middle curve is the total cross section; and the lower is $4\pi \cdot \sigma(90^\circ)$. (Illustrated in the first figure by A, B, and C, respectively.) In all cases the exchange dependence is assumed to be $\frac{1}{2}(1 + P_x)$ (therefore, $\sigma(180^\circ) = \sigma(0^\circ)$), and the depths are chosen to fit the deuteron and the zero energy scattering.

13854 - 1

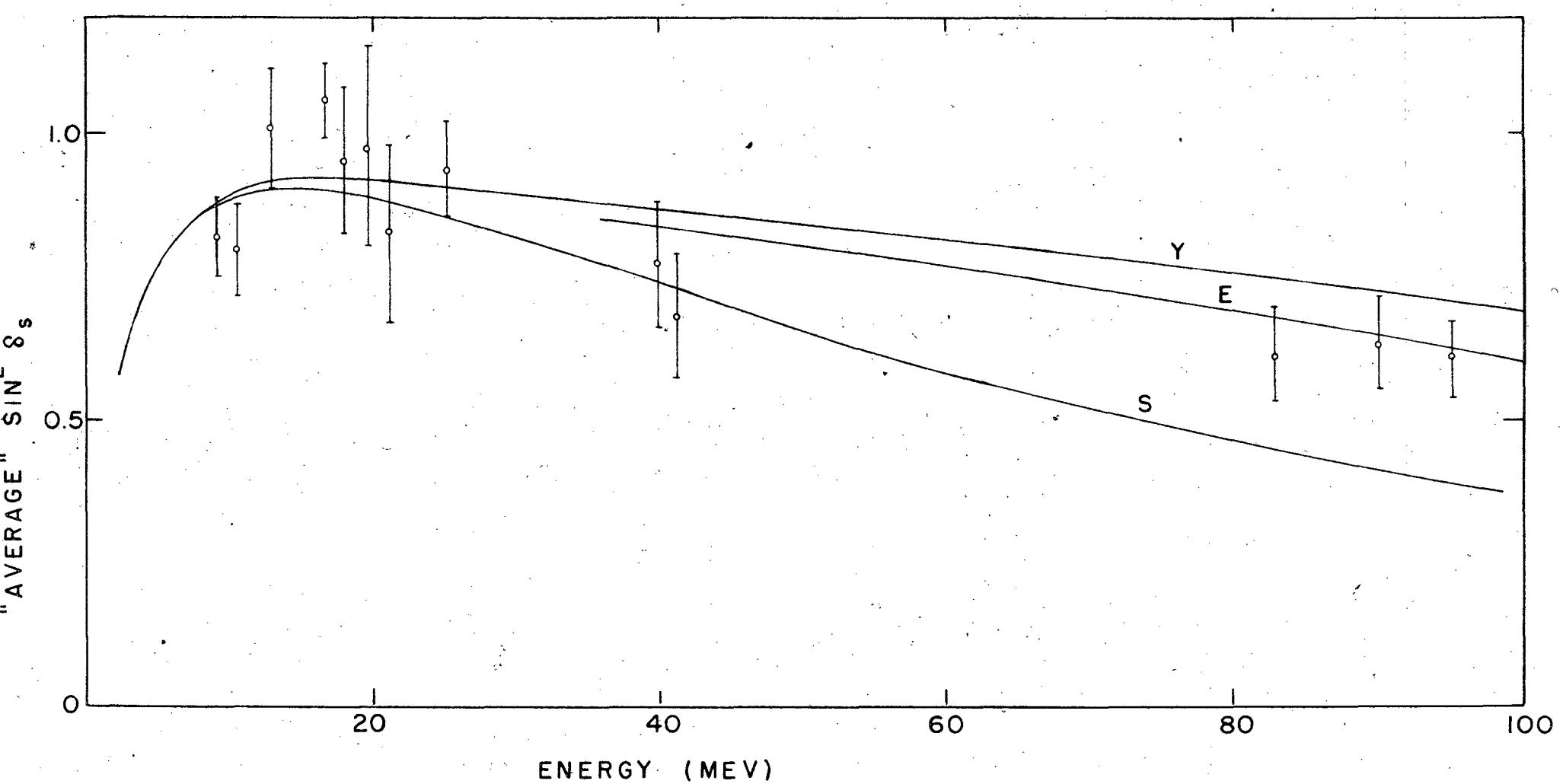

Figure 7

S-wave scattering cross section, illustrated for a triplet effective range of 1.65×10^{-13} cm and a singlet effective range of 3.0×10^{-13} cm. Y, E, and S refer to the Yukawa, exponential and square well central potentials, respectively. The experimental points below 25 Mev are from the data of Sleator[18] and Sherr[19] (above 40 Mev, cf. Table 2).

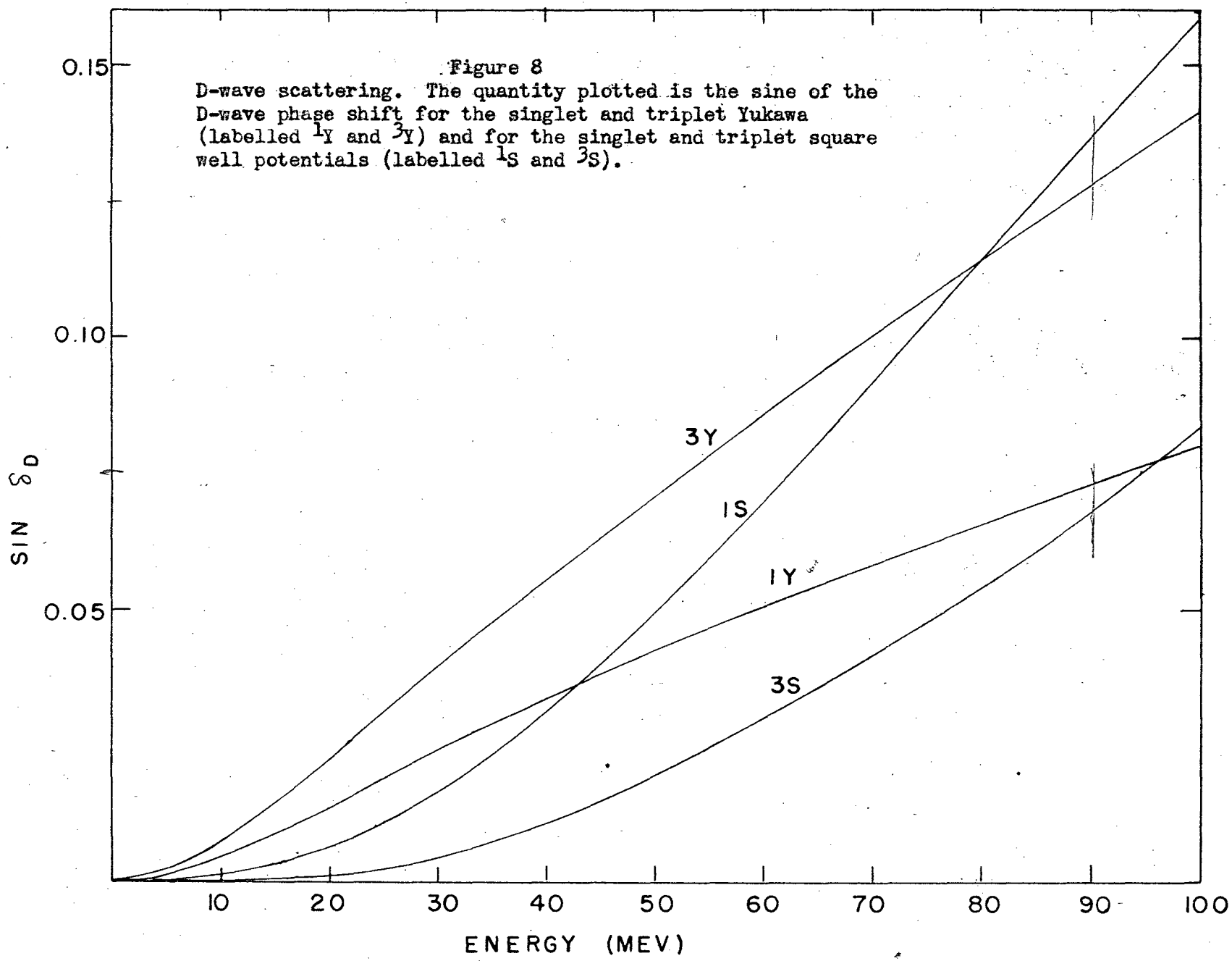

Figure 8
D-wave scattering. The quantity plotted is the sine of the D-wave phase shift for the singlet and triplet Yukawa (labelled ^1Y and ^3Y) and for the singlet and triplet square well potentials (labelled ^1S and ^3S).

13856-1

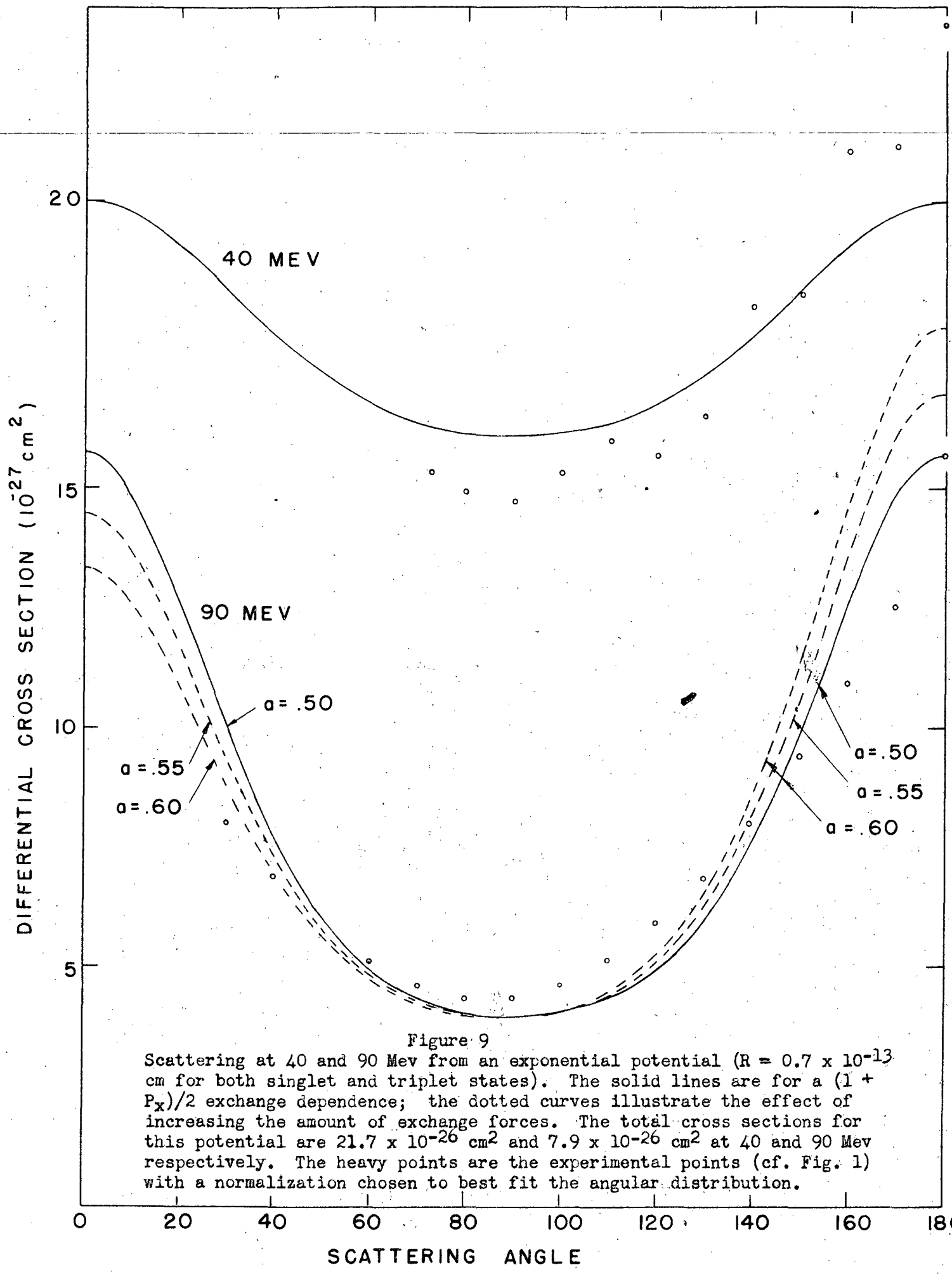

Figure 9

Scattering at 40 and 90 Mev from an exponential potential ($R = 0.7 \times 10^{-13}$ cm for both singlet and triplet states). The solid lines are for a $(1 + P_x)/2$ exchange dependence; the dotted curves illustrate the effect of increasing the amount of exchange forces. The total cross sections for this potential are 21.7×10^{-26} cm^2 and 7.9×10^{-26} cm^2 at 40 and 90 Mev respectively. The heavy points are the experimental points (cf. Fig. 1) with a normalization chosen to best fit the angular distribution.

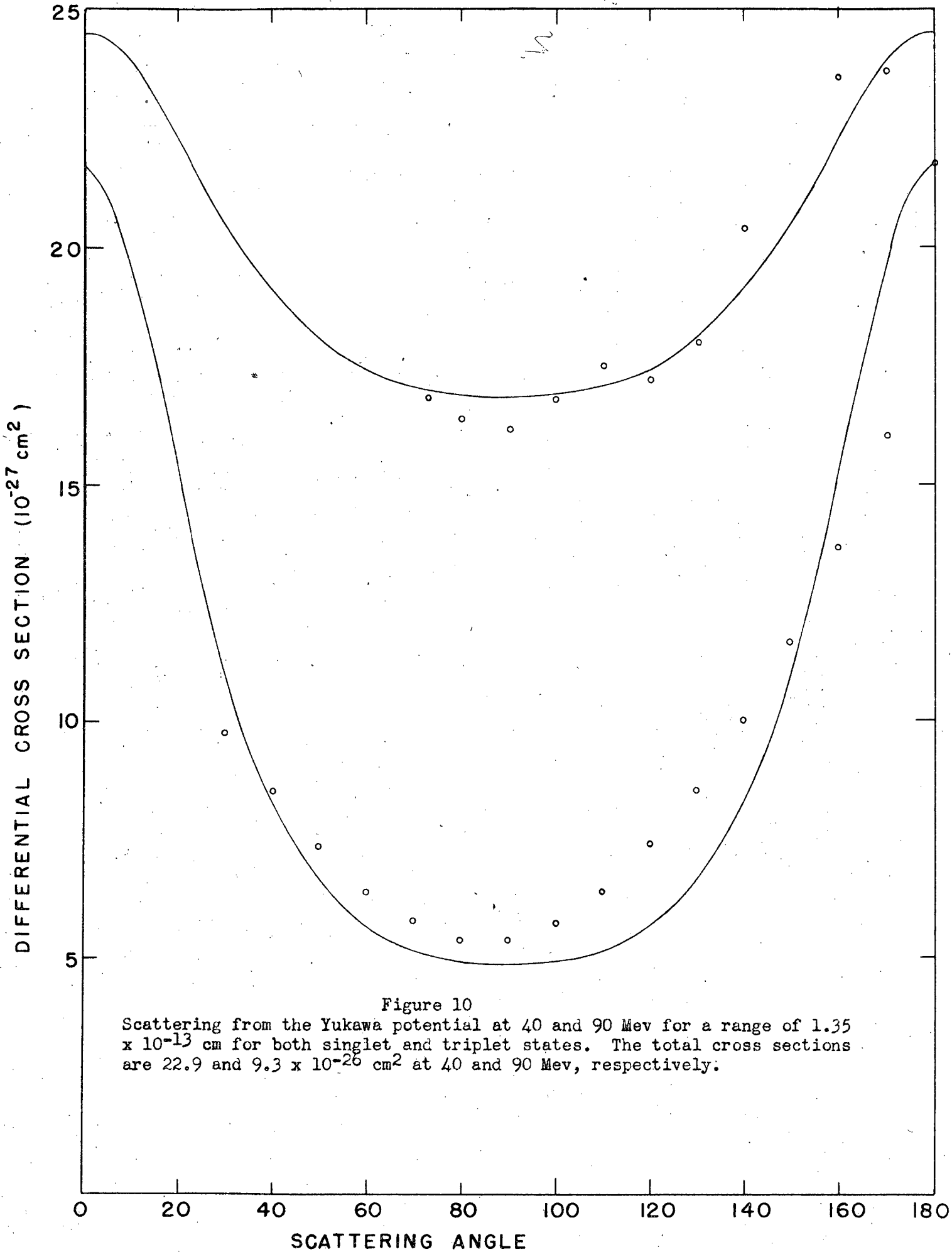

Figure 10
Scattering from the Yukawa potential at 40 and 90 Mev for a range of 1.35 x 10^{-13} cm for both singlet and triplet states. The total cross sections are 22.9 and 9.3 x 10^{-26} cm^2 at 40 and 90 Mev, respectively.

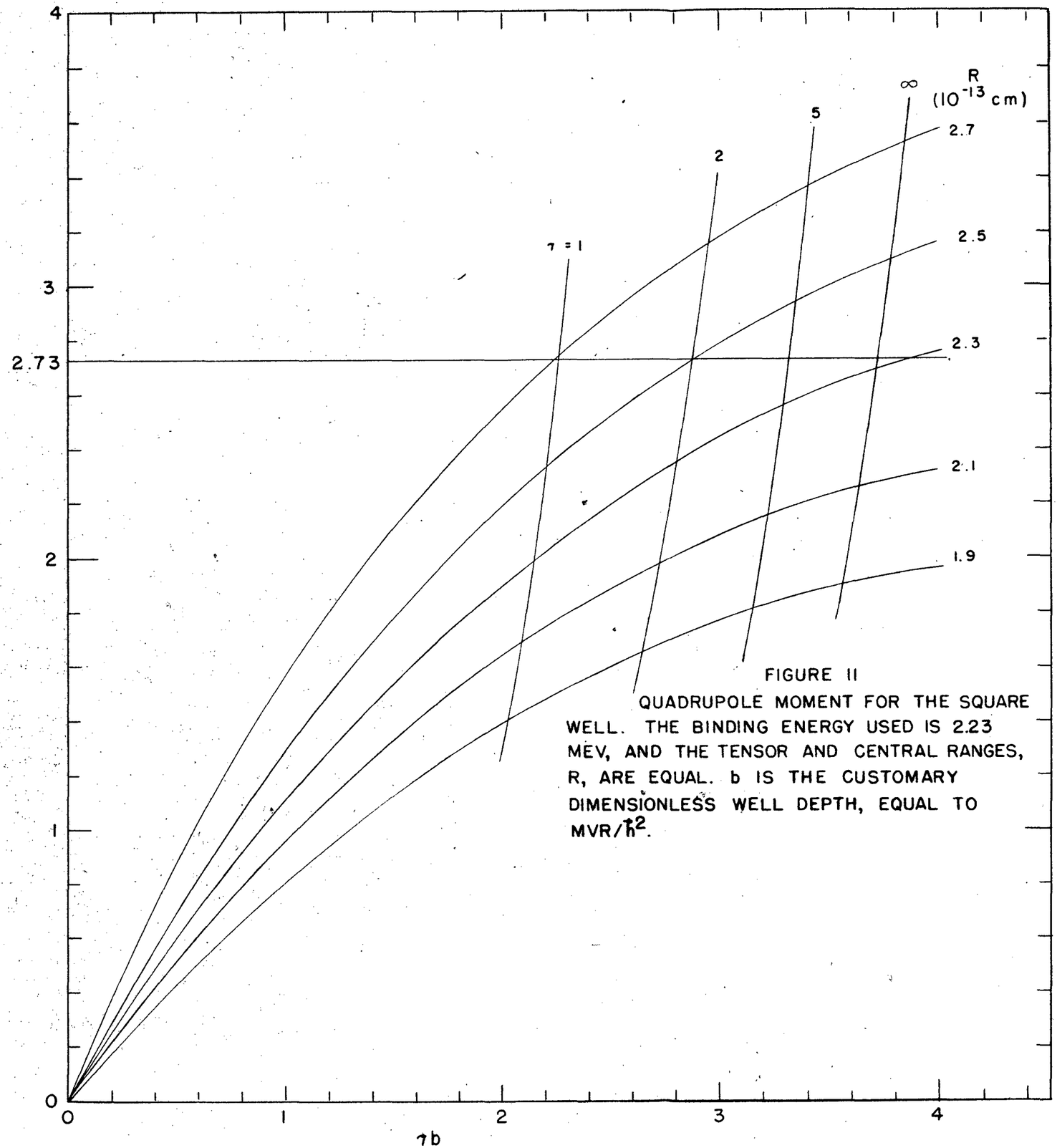

FIGURE II

QUADRUPOLE MOMENT FOR THE SQUARE WELL. THE BINDING ENERGY USED IS 2.23 MEV, AND THE TENSOR AND CENTRAL RANGES, R, ARE EQUAL. b IS THE CUSTOMARY DIMENSIONLESS WELL DEPTH, EQUAL TO $MVR/\hbar^2$.

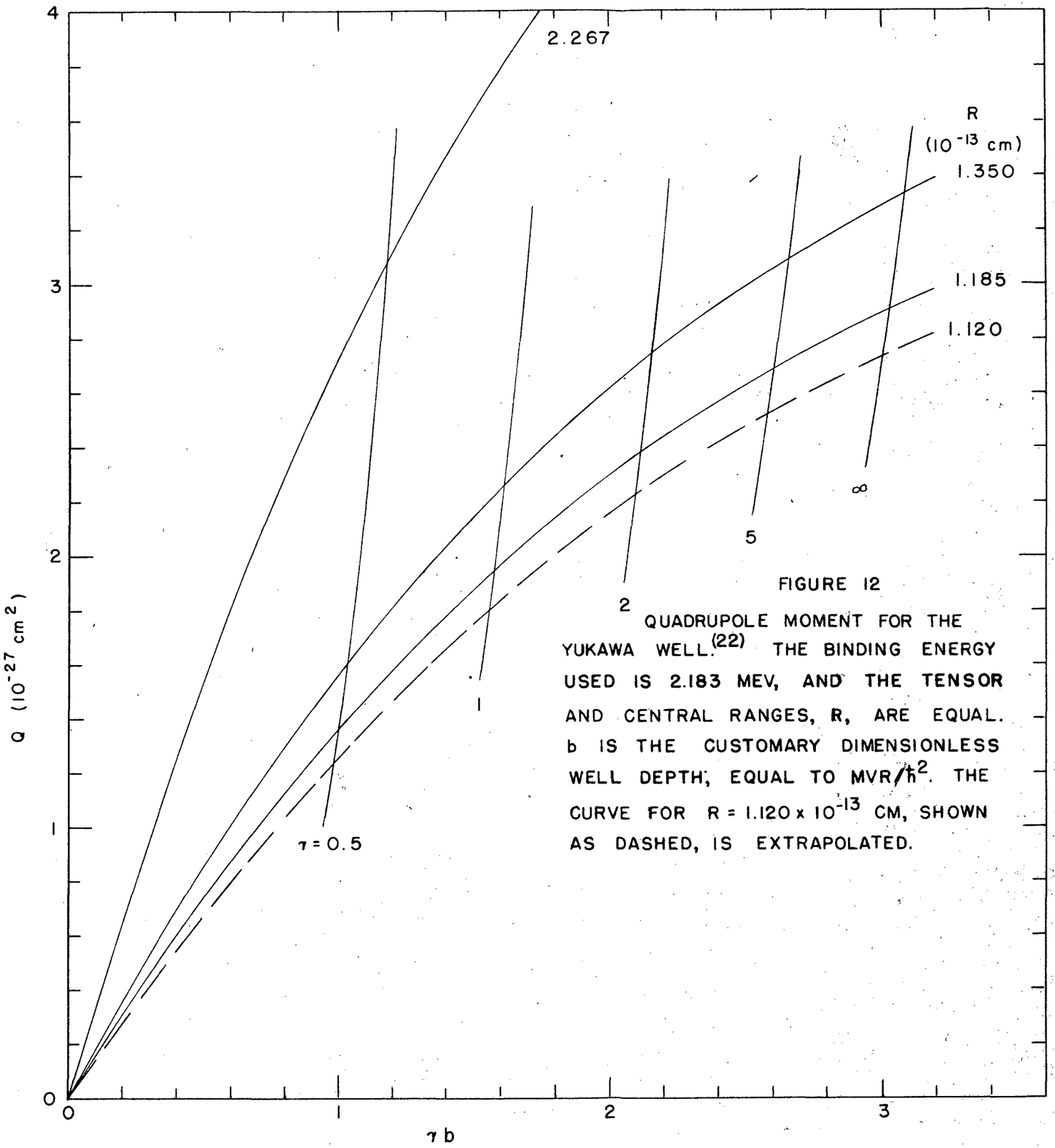

FIGURE 12

QUADRUPOLE MOMENT FOR THE YUKAWA WELL.[22] THE BINDING ENERGY USED IS 2.183 MEV, AND THE TENSOR AND CENTRAL RANGES, R, ARE EQUAL. b IS THE CUSTOMARY DIMENSIONLESS WELL DEPTH, EQUAL TO $MVR/\hbar^2$. THE CURVE FOR $R = 1.120 \times 10^{-13}$ CM, SHOWN AS DASHED, IS EXTRAPOLATED.

13860-2

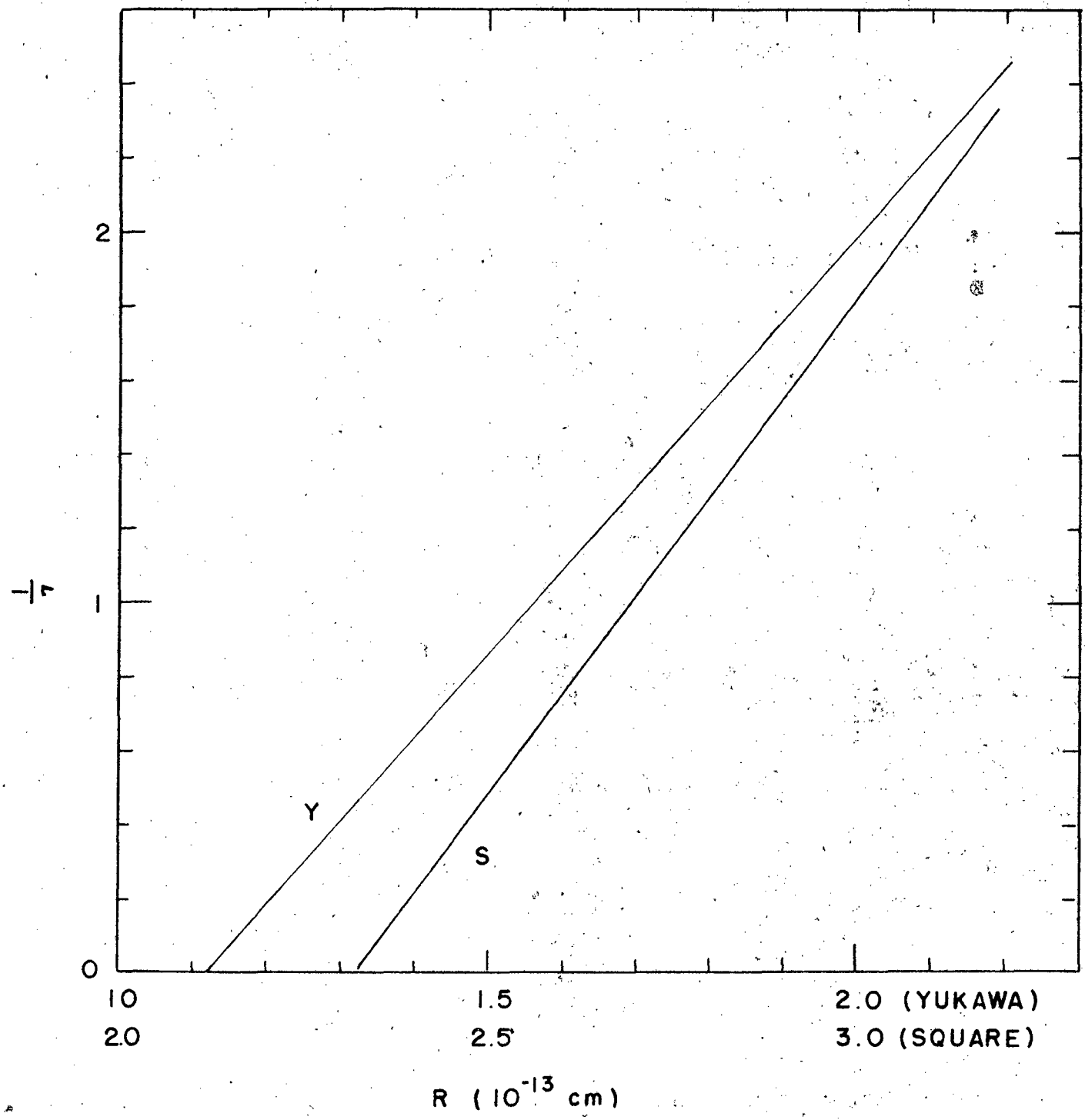

Figure 13
Ratio of central well depth to tensor well depth for quadrupole moment equal to 2.73×10^{-27} cm^2. The binding energy fitted for the Yukawa (Y) case is 2.183 Mev and for the square well (S) case is 2.83 Mev.

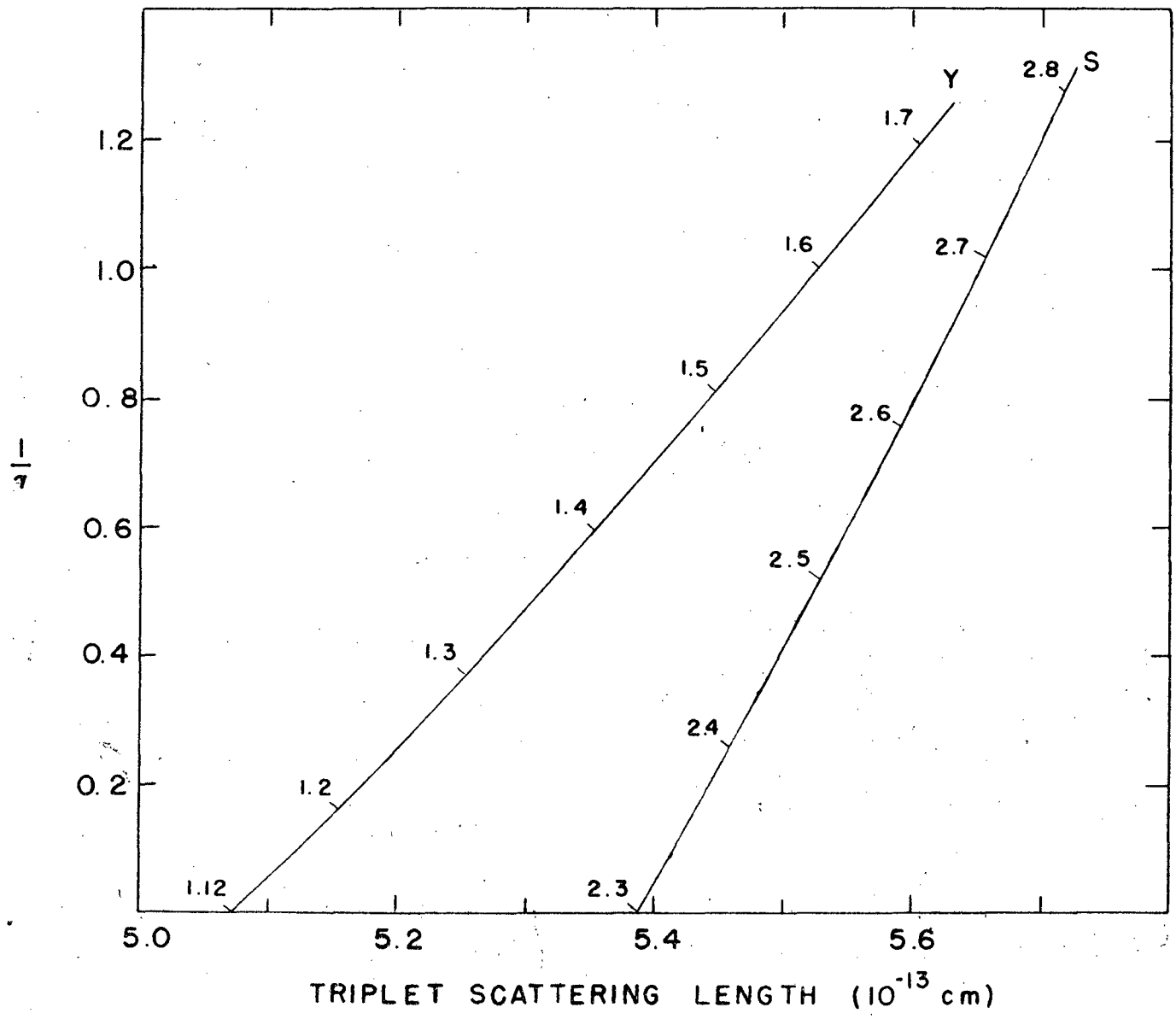

Figure 14

Low energy scattering with tensor forces for the Yukawa (Y) and the square well (S) potentials. The range is indicated (in units of 10^{-13}cm) parametrically along the curves. (Depths are adjusted to fit the binding energy and the quadrupole moment of the deuteron).

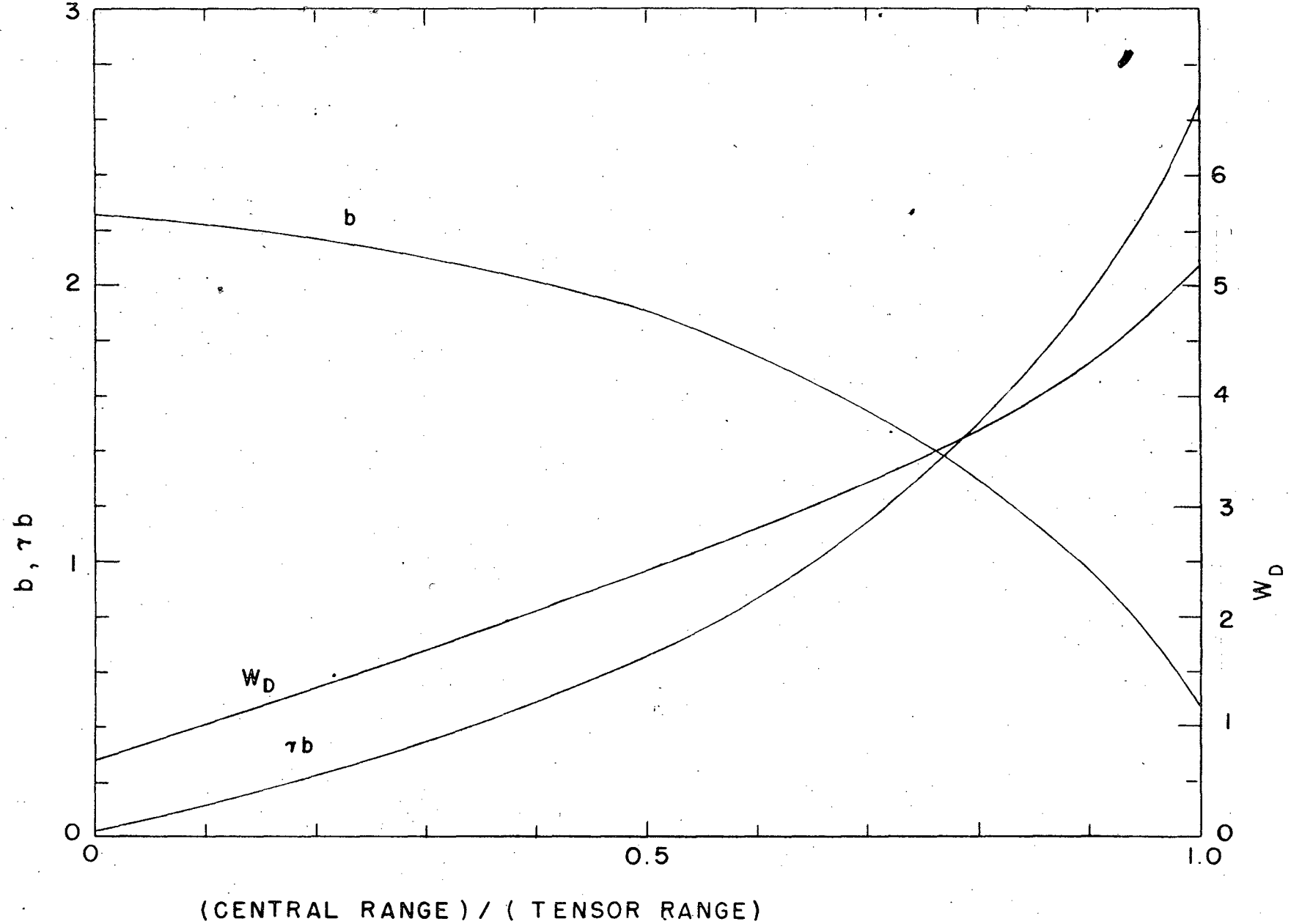

Figure 15

Variation of deuteron fitting parameters for increase of tensor range. The interaction is that of the Yukawa well for which the central range is 1.185×10^{-13} cm. W_D is the percentage of D state; b is the dimensionless central well depth equal to $MVR^2/\hbar^2$; γb is the tensor well depth. The binding energy fitted is 2.183 Mev.

13863-1

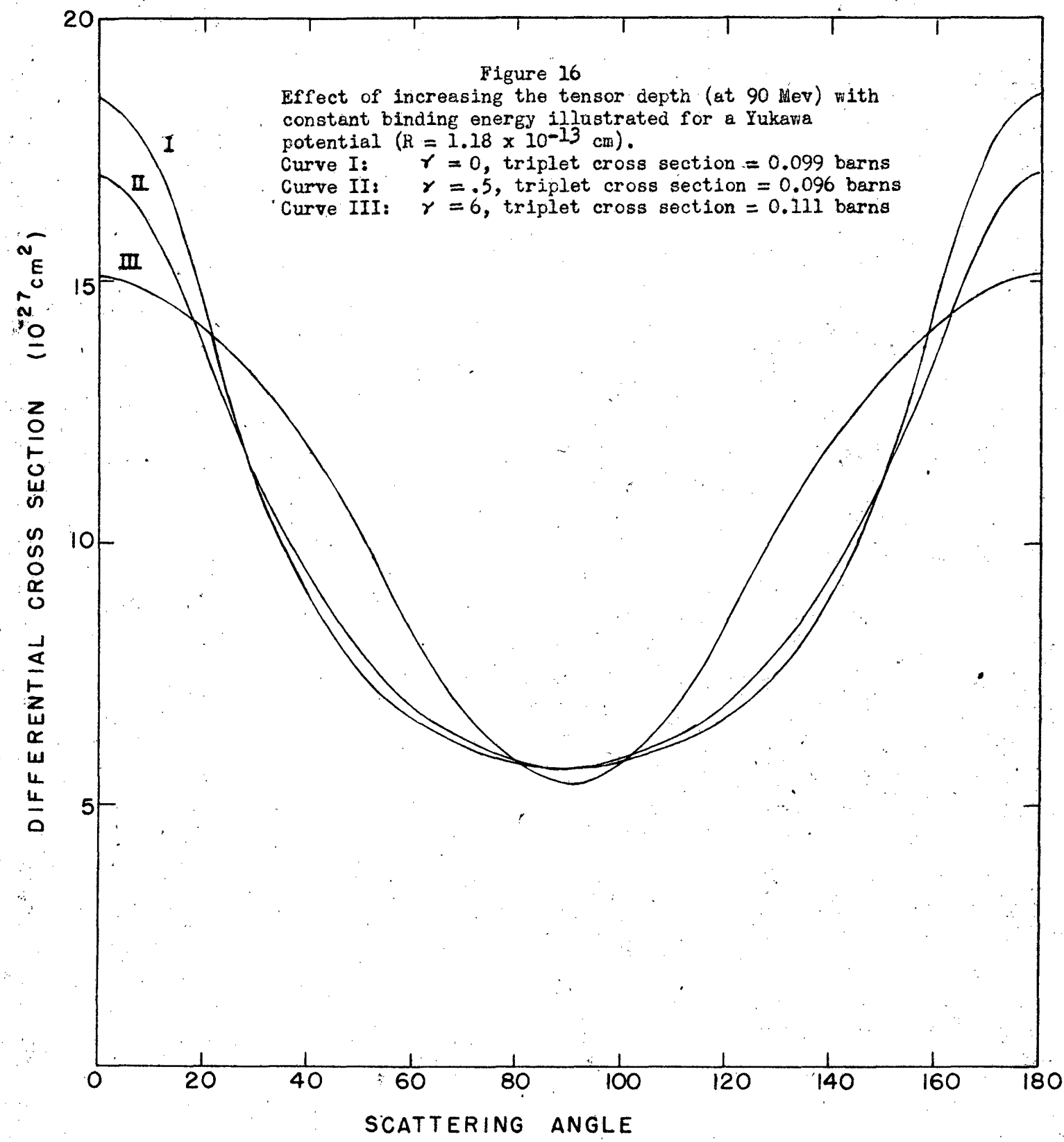

Figure 16
Effect of increasing the tensor depth (at 90 Mev) with constant binding energy illustrated for a Yukawa potential ($R = 1.18 \times 10^{-13}$ cm).
Curve I: $\gamma = 0$, triplet cross section = 0.099 barns
Curve II: $\gamma = .5$, triplet cross section = 0.096 barns
Curve III: $\gamma = 6$, triplet cross section = 0.111 barns

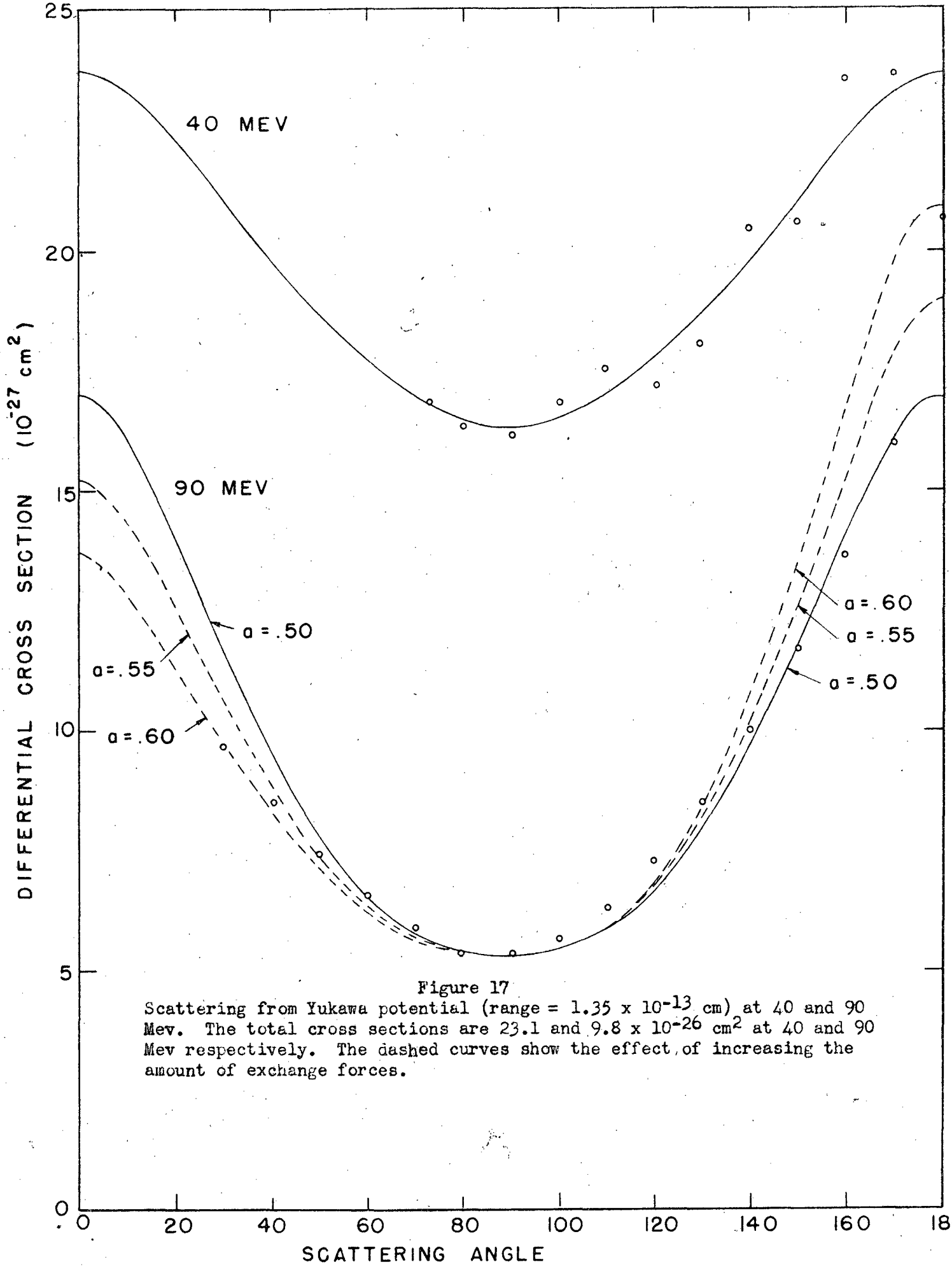

Figure 17
Scattering from Yukawa potential (range = 1.35×10^{-13} cm) at 40 and 90 Mev. The total cross sections are 23.1 and 9.8×10^{-26} cm^2 at 40 and 90 Mev respectively. The dashed curves show the effect of increasing the amount of exchange forces.

13865-1

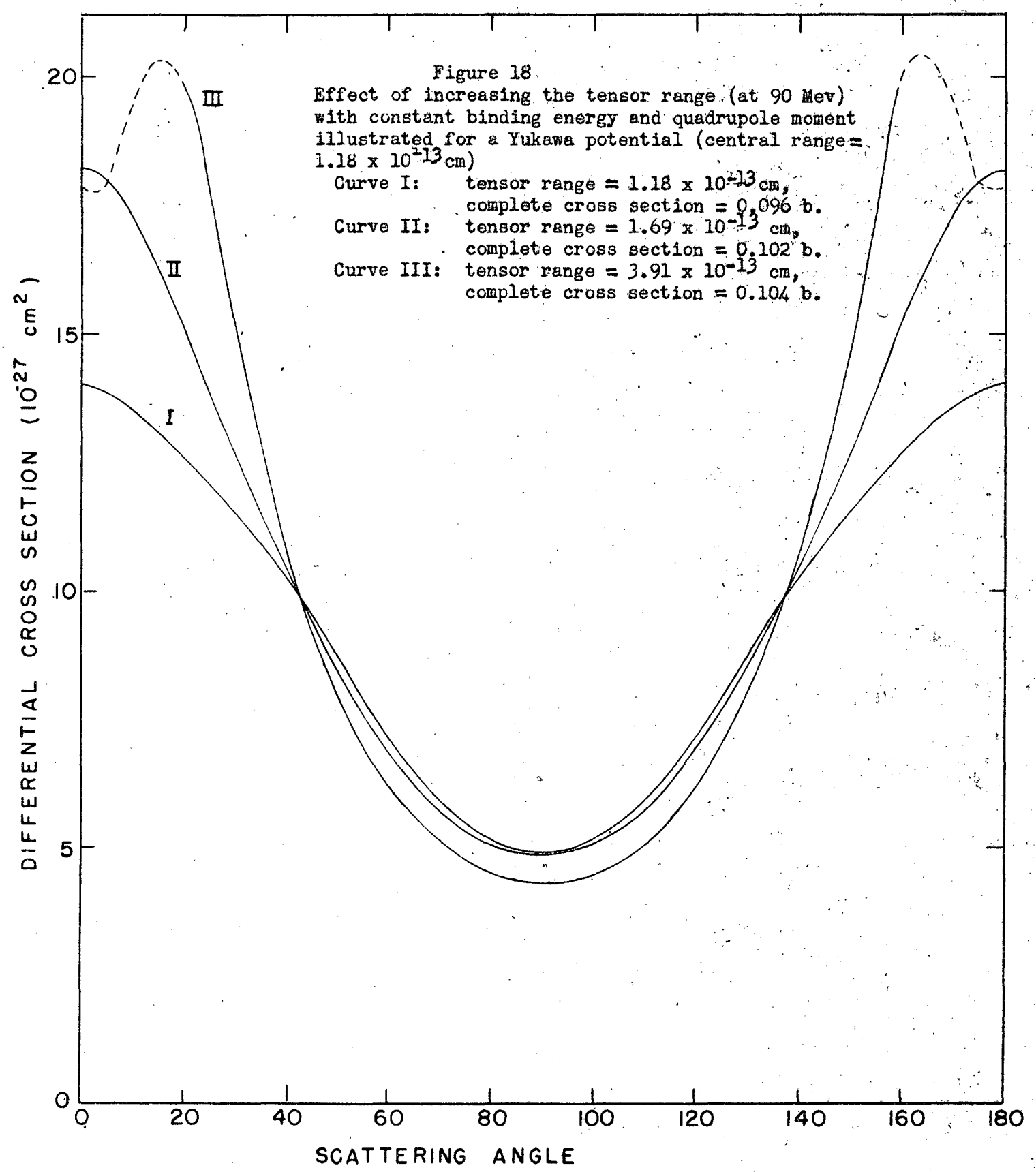

Figure 18
Effect of increasing the tensor range (at 90 Mev) with constant binding energy and quadrupole moment illustrated for a Yukawa potential (central range = 1.18×10^{-13} cm)

Curve I: tensor range = 1.18×10^{-13} cm, complete cross section = 0.096 b.

Curve II: tensor range = 1.69×10^{-13} cm, complete cross section = 0.102 b.

Curve III: tensor range = 3.91×10^{-13} cm, complete cross section = 0.104 b.